Journal of Power Sources 195 (2010) 2319–2330

Contents lists available at ScienceDirect

Journal of Power Sources

journal homepage: www.elsevier.com/locate/jpowsour

An impedance study of an operating direct methanol fuel cell

Shu-Han Yang[a,*], Charn-Ying Chen[b], Wen-June Wang[a,c]

[a] Department of Electrical Engineering, National Central University, Jhong-li, 320, Taiwan
[b] Institute of Nuclear Energy Research (INER), Longtan, Taoyuan, 325, Taiwan
[c] Department of Electrical Engineering, National Taipei University of Technology, Taipei, Taiwan

ARTICLE INFO

Article history:
Received 11 September 2009
Received in revised form 22 October 2009
Accepted 22 October 2009
Available online 31 October 2009

Keywords:
Direct methanol fuel cell
Electrochemical impedance spectroscopy
Pseudo-dynamic hydrogen electrode
Charge-transfer resistance (CTR)

ABSTRACT

An electrochemical impedance spectroscopy (EIS) technique was developed to characterize a direct methanol fuel cell (DMFC) under various operating conditions. A silver/silver chloride electrode was used as an external reference electrode to probe the anode and cathode during fuel cell operation and the results were compared to the conventional anode or cathode half-cell performance measurement using a hydrogen electrode as both the counter and reference electrode. The external reference was sensitive to the anode and the cathode as current was passed in a working DMFC. The impedance spectra and DMFC polarization curves were systematically investigated as a function of air and methanol flow rates, methanol concentration, temperature, and current density. Water flooding in the cathode was also examined.

1. Introduction

Direct methanol fuel cells (DMFCs) would be highly desirable for powering portable electronic devices because they would offer several attractive advantages, such as ease of fuel storage, low operating temperature, and high energy density [1–10]. The cell performance depends on the membrane-electrode assembly (MEA), which comprises a polymer electrolyte membrane, a catalyst layer, and a gas-diffusion layer. The DMFC has not yet found widespread commercial application because MEA performance, durability, and long-term operation are limited, mainly due to low anode-electrocatalyst activity as well as fuel-crossover issues.

Electrochemical impedance spectroscopy (EIS) has long been utilized to probe interfacial processes and speciation in electrochemical systems. EIS data are often presented as a Nyquist plot in which, ideally, the leftmost intercept with the real (*X*-axis) occurs for the high-frequency data, which is related to the ohmic resistance of the cell elements (the sum of the membrane, electrodes, contacts, and other resistances) and is named high-frequency resistance (HFR). The next real axis intercept, which is further to the right (lower-frequency data), is related to the charge-transfer resistance (CTR) for the faster charge-transfer reaction on one of the two electrodes. The last real axis intercept is further to the right (lowest-frequency data) and indicates the CTR of the slower reaction on the other of the two electrodes. EIS studies of DMFCs under various test conditions, such as a large electrode area, high temperature, and large DC current, have been recently performed [2–26]. The most common method for distinguishing the individual impedances of the anode and the cathode from the full cell is to use a dynamic hydrogen electrode (DHE) as both the counter and reference electrodes [2–6,9–15,18,19,21,24,27]. The anode impedance can be obtained by measuring the full-cell impedance with a hydrogen [4] stream, instead of air or oxygen, passing over a cathode. Then the cathode impedance is extracted by subtracting the anode impedance from the full-cell impedance associated with the overall reaction. Notably, the HFR of the cathode impedance will be incorporated into the HFR of the anode impedance during the calculation because the anode impedance is measured in the form of a full cell using a half-cell reaction. However, the pseudo-DHE possibly exhibits overpotential due to impurities such as O_2. In some investigations, the methanol solution was replaced with sulfuric acid to determine the cathode impedance alone, or sulfuric acid was streamed into the cathode to investigate the anode impedance [8,20,22,23,26]. Nevertheless, these methods consider only an ideal situation, not a real electrode environment. Although the impedance of a real anode and a real cathode in the discharge regime can be resolved by an additional dynamic hydrogen electrode [27–32] or by a reversible hydrogen electrode [33–35], the appended structure of the reference electrode for an H_2 stream increases the complexity of cell construction.

This work overcomes the difficulties associated with the above-described methods by using an independent structure for a reference electrode. An Ag/AgCl electrode was first used as a reference electrode with minimal instability to observe the impedance of each electrode. The unique advantages of this reference electrode

* Corresponding author at: Department of Electrical Engineering, National Central University, Jhong-li, 320, Taiwan. Tel.: +886 3 4227151x34562; fax: +886 3 4255830.
E-mail address: kalodolum@anet.net.tw (S.-H. Yang).

0378-7753/$ – see front matter © 2009 Elsevier B.V. All rights reserved.
doi:10.1016/j.jpowsour.2009.10.066

are that it can avoid the effect of impurities such as O_2 and can be easily applied in the electrochemical system. Moreover, the accuracy of the determinations of the individual electrode impedances is ensured by comparing the summation of the real-anode and real-cathode impedances with the full-cell impedance. By this extended method, the EIS response of the real anode, the real cathode, and the full-cell impedance were determined together with the polarization curves under various operating conditions. Additionally, the real-anode impedance was compared with the half-cell impedance of the anode under the same operating conditions to show the advantage of the proposed approach.

2. Experimental

2.1. Fabrication of membrane-electrode assembly

The MEAs, consisting of electrodes and electrolyte membranes, were prepared by the procedure reported in our previous work [16,17]. The catalysts were purchased form Johnson Matthey Inc. The electrode inks were fabricated from a mixture of Pt–Ru/C or Pt/C catalysts with a Nafion solution (DuPont). Nafion 117 membranes were cleansed in turn in deionized water, 3 wt.% H_2O_2, 3 wt.% H_2SO_4, and deionized water again for 1 h in each solution. A thin layer of electrode with the above catalyst was then coated onto each surface of the cleansed membrane by a screen-printing technique. Pt–Ru and Pt were deposited onto the anode and cathode, respectively, both at a loading rate of 2 mg cm^{-2} [38,39,43]. After hot-pressing at 120 °C and 50 kg cm^{-2} for 2 min, the active area of the MEA was aligned to 25 cm^2 using a laser-ablation process [43]. A Nd-yttrium aluminum-garnet laser was utilized at a wavelength of 1065 nm. The probe chuck of the focus of the fixed laser optics was movable in the x–y plane with an accuracy of 1 μm at a speed of 200 mm s^{-1}. The lowest possible pulse-energy density of 0.25 J cm^{-2}, with a high-pulse frequency of 20 kHz, was selected to avoid local overheating of the membrane. The MEA was covered with a glass substrate and a silicon mask was placed on top of the glass substrate to absorb the initial energy of the laser. The laser started and stopped on the Si mask. During the laser-ablation process, the redundant catalyst of both anode and cathode was evaporated or adhered to the glass substrate. The influence of the asymmetric potential distribution on the working electrode was thereby minimized. Subsequently, the MEA was installed in a test block with the current collectors positioned at each end and then sandwiched between gas-diffusion layers. The carbon cloth treated with 5 wt.% PTEF was used as the gas-diffusion layer (GDL) for both anode and cathode with the thickness of 0.29 mm. A carbon cloth treated with 5 wt.% PTEF was used as the gas-diffusion layer (GDL) for both anode and cathode, with a thickness of 0.29 mm. The gasket thickness of both the anode side and cathode side was 0.2 mm. Channels with parallel geometry (1 mm wide, 1.2 mm deep, with ridges 1 mm high) were machined in the plates.

2.2. Single-cell operation

A thermocouple was used to monitor and control the desired cell temperature. A 3-wt.% methanol solution was fed from a methanol container with a pump and preheated to the operating temperature. The flowmeter was positioned after the valve of the compressor to regulate the air flow at room temperature. A 50-ml min^{-1} flow of hydrogen gas was used for the half-cell impedance of the anode. Before the EIS measurement, the cell was preheated to 60 °C for 1 h without air supply. Then, a load was applied at 40 mA cm^{-2} for 1 h to insure a steady state. The current–voltage (polarization curves) and current–power characteristics were measured galvanostatically with an electronic loader (Prodigit 3300C).

2.3. Electrochemical measurements

The impedance spectra were recorded with a ZAHNER IM 6ex instrument (equipped with four measuring electrodes, a working electrode (WE), a sensing electrode (SE), a reference electrode (RE), and a counter-electrode (CE)), allowing measurement of the modulation of DC potential in automatic sweep mode from 1 kHz to 0.05 Hz with 10 steps per logarithmic decade. The amplitude of the sinusoidal modulation voltage did not exceed 10 mV. In addition to the usual cell hardware, the Ag/AgCl electrode (MF-2052, BAS Inc.) was inserted into the cell through openings in the end plates to contact the region of constant potential (RCP; 1.5 times the membrane thickness beyond the electrode edge) [38,39,43] and fixed in place by means of plastic compression fittings to ensure electrical isolation of the reference electrode from the holes in the end plates, as shown in Fig. 1. The periphery around the contact position of the membrane was treated with Si-Fluoro elastomer (Topco Scientific Co.) to prevent chloride ions leakage from the Ag/AgCl electrode, which would poison the catalyst [40–42], and to ensure a continuous path for chloride ions between the reference electrode and the membrane surface.

In order to evaluate the stability of the Ag/AgCl reference electrode, the individual potential was periodically measured at the normal DMFC open-circuit condition for ~3.8 h (Fig. 2(a)) and again at a constant current density of 100 mA cm^{-2} for ~3.8 h (Fig. 2(b)). As the cathode potential was measured from the reference, R_A, the resistance of membrane might cause a slight potential drift and result in a different cathode potential between the V_C (from the reference R_A) and the $V_{cathode}$ (from the reference R_C). Furthermore, the repeated reference-electrode response of anode and cathode indicated good stability of the reference electrode during fuel cell operation [38]. The trend of stability of the individual potential measurements was also observed during the polarization measurements over all of the current densities, as shown in Fig. 2(c).

All of the in situ EIS were carried out based on the reference electrode, R_A. The connection forms for the in situ EIS measurement are plotted in Fig. 3. To verify the accuracy of the EIS measurement, Figs. 4 and 5, respectively, show the EIS during the half-cell reaction and the actual operation. For measurement of the half-cell impedance of the anode (Fig. 4), the cathode electrode was operated as a DHE. Clearly, the real high-frequency resistance (HFR) of the anode can be isolated by using the Ag/AgCl. Furthermore, the charge-transfer resistances (CTR) of each electrode, as well as the individual HFR, were separated during operation of the different airflows of 100 and 300 ml min^{-1}, as plotted in Fig. 5(a) and (b). As a result, the summation of the individual anode and cathode impedances (Fig. 5 (c) and (d)) is consistent with the full-cell impedance. This result indicates that the potential at the edge of an electrode versus the reference followed the electrode potential.

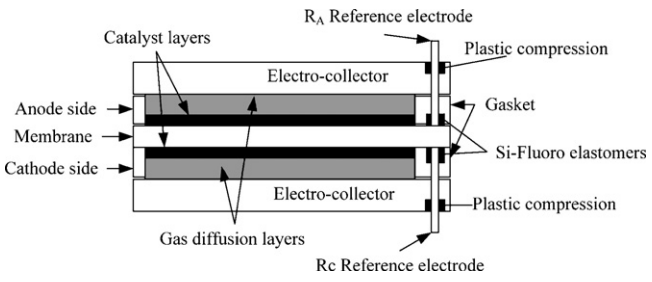

Fig. 1. Cell configurations.

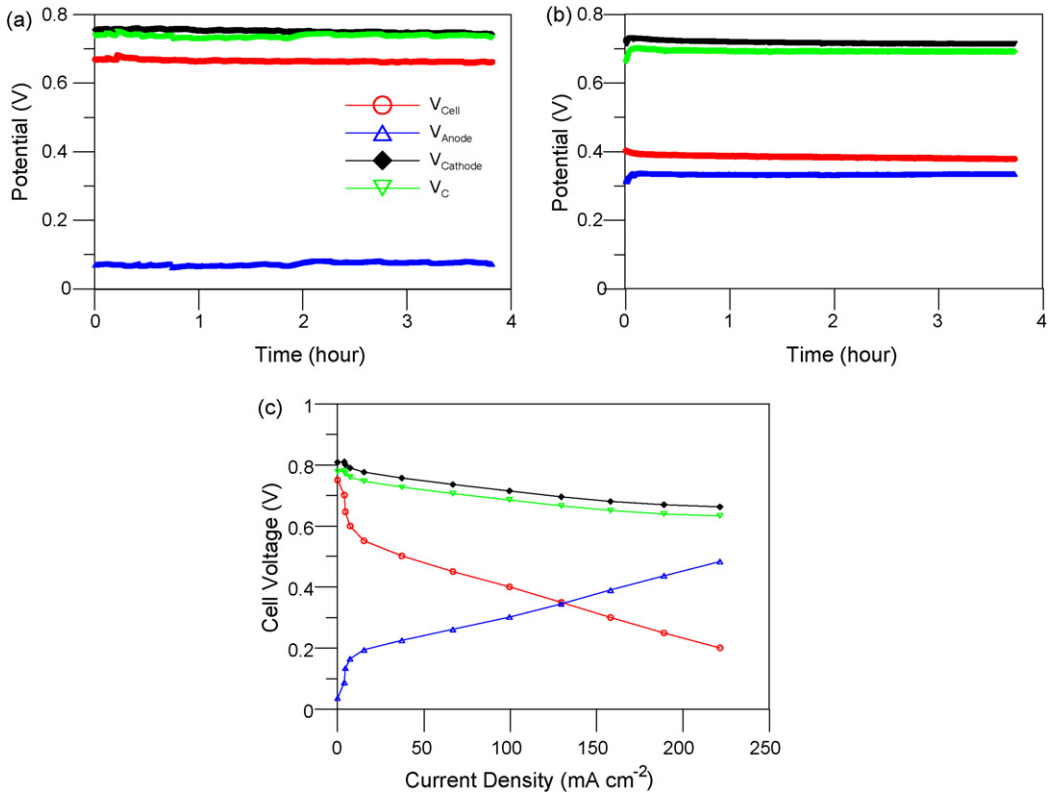

Fig. 2. The individual potential measurement by using Ag/AgCl at (a) open-circuit voltage, (b) a constant current density of 100 mA cm^{-2}, and (c) the polarization curves. The V_{cell} is the full cell potential. V_{anode} is the anode potential measured from the reference R_A. $V_{cathode}$ is the cathode potential measured from the reference R_A. $V_{cathode}$ is the cathode potential measured from the reference R_C.

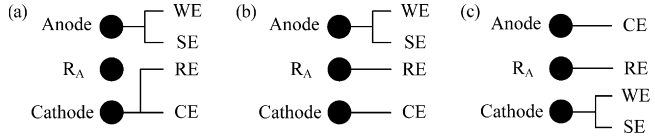

Fig. 3. The connections of the electrodes for measuring the impedance of (a) full cell, (b) anode, and (c) cathode.

2.4. Effect of chloride ions on EIS measurement

Although a minimal amount of chloride ion leakage resulted from sealing of the Ag/AgCl electrode in the path between the reference and membrane surfaces by use of the Si-Fluoro elastomer (Topco Scientific Co.), it is possible that some chloride ions diffused through the membrane and directly poisoned the catalyst. Therefore, it was necessary to ensure elimination of the chloride poison in our experiment [41]. During the roughly 8-h operation, the concentrations of chloride ions originating from the anode and cathode outlet were measured by inductively coupled plasma (ICP) mass spectrometry, as shown in Fig. 6. After the 8-h operation, the chloride ions adsorbed on the anode and cathode catalyst were present at levels (see Table 1) below the detection limit of energy-dispersive X-ray (EDX) analysis. These results indicate that the minimal leakage of chloride ions from the Ag/AgCl reference did not affect the accuracy of the EIS measurement in our work.

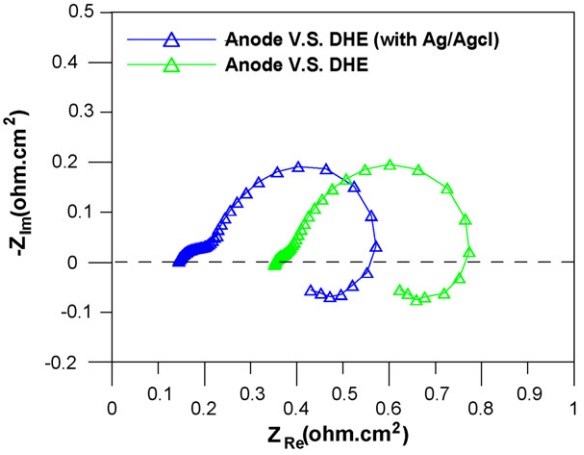

Fig. 4. Comparisons of the two different half-cell impedance of anode (measured against DHE).

3. Results and discussions

3.1. Effect of air flow rates

Three air flow rates, corresponding to cathode stoichiometries of 1, 3 and 9, were set at a constant current of 76 mA cm^{-2}. The stoichiometric flow rate of the anode was set to 6 when a 3-wt.%

Table 1
EDX patterns of the catalysts.

Anode			Cathode		
Element	wt.%	at.%	Element	wt.%	at.%
C K	32.20	60.45	C K	36.59	65.29
O K	4.84	6.83	O K	3.77	5.05
F K	22.05	26.17	F K	21.89	24.70
S K	0.89	0.63	S K	1.19	0.79
Ru L	12.16	2.71	Ru L	1.49	0.32
Pt M	27.87	3.22	Pt M	35.07	3.85

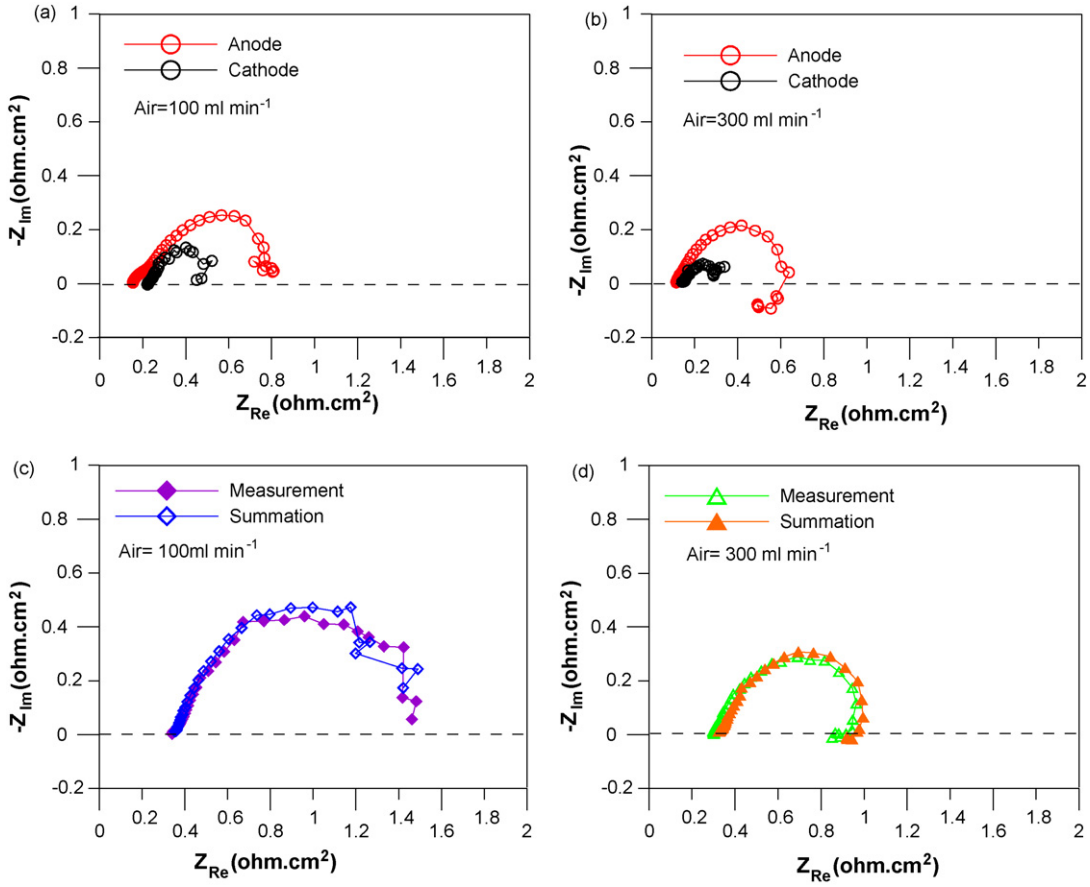

Fig. 5. Nyquist plots for a DMFC at 76 mA cm^{-2} with (a and c) 100 ml min^{-1} air flow and (b and d) 300 ml min^{-1} air flow. Cell temperature is 60 °C, liquid methanol flow is 6-stoichiometry.

methanol solution was used at 60 °C. The electrochemical behavior of the real cathode under various air flow rates is recorded in Fig. 7(a). At a cathode stoichiometry of 1, the oxygen mass-transport limitation yielded a large irregular semicircle for the real-cathode impedance. When the oxygen mass transport (concentration) is increased, the oxygen-reduction reaction (ORR) is enhanced, which reduces the CTR of the cathode impedance as well as the irregular shape in the low-frequency region. Regarding the real-cathode EIS, Fig. 7(b) plots the electrochemical behavior of the real anode. Interestingly, the irregular shape resulting from the mass-diffusion problem was also observed in the low-frequency region of the real-anode EIS at an anode stoichiometric flow rate of 6. In the conventional half-cell EIS of the anode, the diffusion problem generally only occurs because of anodic mass-transport limitations at low fuel-flow rates or concentrations [2,3,7,12]. The anode-diffusion problem remained at a cathode stoichiometry of 3, when the stoichiometric flow rate of methanol supply was sufficient (6 in this study), because the oxygen mass-transfer limitation slows the proton-transfer process from anode to cathode. The observed slowing of proton-transfer is due to the diffusion problem, which then causes the irregular shape of the real-anode EIS. When the stoichiometric flow rate of the supplied air was 9 at the cathode, the proton-transfer process was enhanced, and the irregular shape of the real-anode impedance was almost eliminated. The same result could not be obtained from the half-cell EIS measurement because the fast kinetics and mass transport of the hydrogen oxidation reaction had an undetected influence on the anode impedance during the half-cell reaction. Therefore, similar half-cell impedances of the anode under the various hydrogen flows were demonstrated (Fig. 7(c)). This result indicates that the effect of the cathode on the real anode cannot be identified by determining the half-cell impedance of the anode.

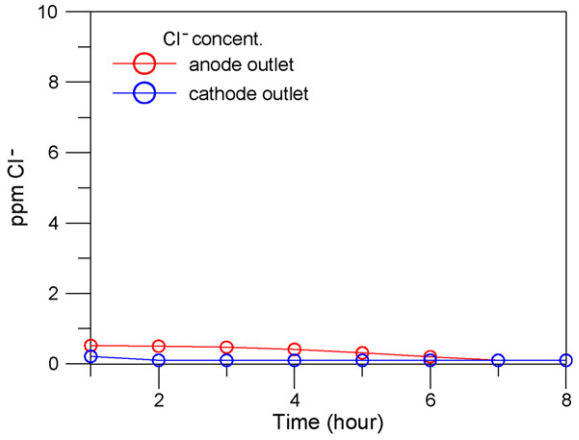

Fig. 6. The concentrations of chloride ions measured from the anode and cathode outlet.

In Fig. 7(d), the resultant effect of both the real anode and the real cathode on the overall reaction was plotted in the form of a full-cell impedance spectrum. At a cathode stoichiometry of 1, the limited ORR slows the proton-transfer process and hence causes the overall reaction to generate a large irregular semicircle of full-cell impedance. As the air flow rate was increased, the full-cell impedance arc decreased because the fast reactions occurred quickly at both the real anode and the real cathode. This result,

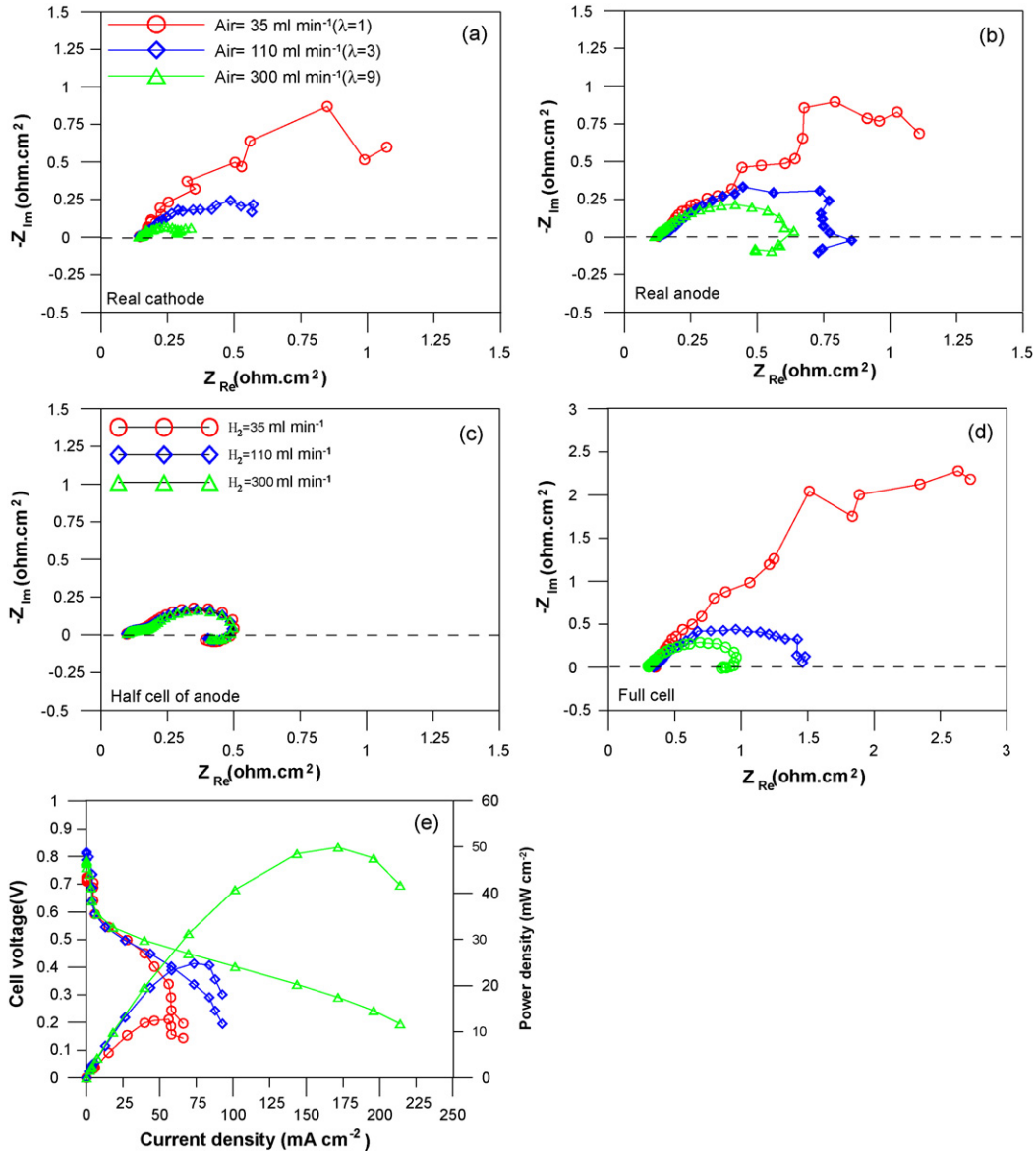

Fig. 7. The influence of 1, 3 and 9 time stoichiometric cathode flow rates on the EIS of (a) real cathode, (b) real anode, (c) half cell of anode, (d) full cell, and (e) polarization curves. Cell temperature is 60 °C, anode flow is 6-stoichiometry.

which is closely related to the polarization curves (Fig. 7(e)), indicates that the air flow rate critically affects the cell performance because of the limited reaction rate at the cathode and the slower proton-transfer process, even with a sufficiently high anode stoichiometry (at least 6). Notably, when the cathode stoichiometry was sufficiently high to eliminate the influence of the oxygen mass-transport limitations, the full-cell impedance clearly exhibited inductive behaviors in the low-frequency region, as shown in Fig. 7(d). The inductive behaviors result from intermediate relaxation of the anode methanol oxidation reaction (MOR), which yields an increase in potential followed by an increase in current with a phase delay, such that the potential-dependent change in capacitance of the full-cell impedance resembles an inductance [3,12].

3.2. *Effect of methanol flow rate*

The influence of the fuel-flow rate was investigated at 76 mA cm^{-2}. Three fuel-flow rates, corresponding to anode stoichiometric rates of 1, 3 and 9, were set using the same methanol concentration of 3 wt.%. The cell was operated at 60 °C with a cathode stoichiometric flow rate of 6. Using the electrochemical characteristics of the real anode, the irregular semicircle was clearly observed at the anode stoichiometry of 1, as shown in Fig. 8(a). In this case, concentration polarization and impaired removal of CO_2 gas bubbles resulted in mass-transport limitations. With an increase of the anode flow, the magnitude of anode impedance decreased along with the reduction of mass-transport limitations. As the fuel stoichiometric rate of the anode was increased to 9, the concentration polarization decreased as well. Simultaneously, the high flow rate accelerated the removal of CO_2, which increased the efficiency of catalyst utilization. Hence, the inductive part appears because the stable MOR produces the intermediate adsorbates on the catalyst surface [12]. The same trend in the variation of anode EIS at the different fuel-flow rates can also be observed in the half-cell impedance of the anode, as shown in Fig. 8(b). At an anode stoichiometric rate of 1, the concentration polarization and the reduction of catalyst utilization efficiency due to excessive CO_2 caused formation of a large impedance arc with an irregular shape in the low-frequency region. When the stoichiometric flow rate of the anode was set at 3, the fast removal of CO_2 and the decreased

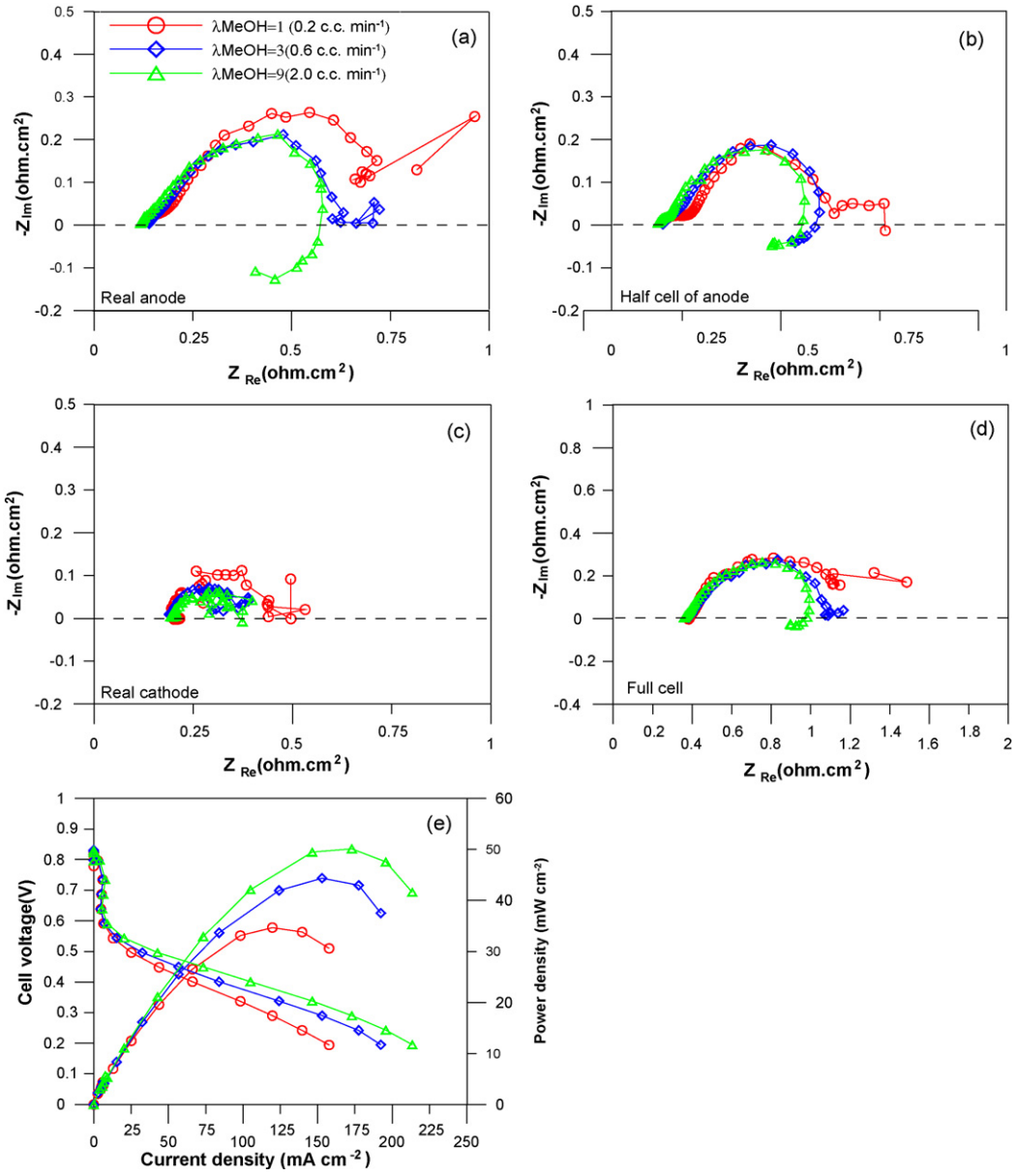

Fig. 8. The influence of 1, 3 and 9 time stoichiometric anode flow rates on the EIS of (a) real anode, (b) half cell of anode, (c) real cathode, (d) full cell, (e) polarization curves. Cell temperature is 60 °C, cathode flow is 6-stoichiometry.

concentration polarization improved the MOR such that the CTR of the half-cell impedance of the anode was reduced, with appearance of the inductive part. A further increase in the anode flow rate had no significant effects.

On the cathode side, Fig. 8(c) shows that the restriction of proton transport due to the low methanol flow reduced the ORR and hence resulted in the large real-cathode impedance arc. In the interim, the CTR decreased with increases in the anode flow rate. Although a high anode flow will increase methanol crossover, the influence of the mixed potential on the ORR was undetectable in this experiment. Taking the full cell impedance into consideration, the electrochemical behaviors associated with the polarization curves (Fig. 8(e)) were investigated, as shown in Fig. 8(d). The poor cell performance (Fig. 8(e)) resulting from the summing effect of both the impaired MOR and suppressed ORR yielded the large, irregular semicircle of the full-cell EIS (Fig. 8(d)) at an anode stoichiometry of 1. As the anode flow rate was increased, the cell performance improved at high current density (76 mA cm^{-2}) due to the decreased concentration polarization and the high efficiency of catalyst utilization. This, in turn, reduced the CTR of the full-cell impedance. At an anode stoichiometric flow rate of 9, no significant differences in the other impedance measurements was observed, except for slight variations in mass transport at low frequency. The results corresponding to these polarization curves indicate that cell performance increased slightly as the anode flow rate increased from 3 to 9 (Fig. 8(e)). Furthermore, performance was not influenced as significantly by the flow rate of methanol as by that of the air, as is clearly indicated by the steep (Fig. 7(e)) and moderate rises in peak power (Fig. 8(e)) for their increases.

3.3. *Effect of methanol concentration*

The influence of methanol concentration (1, 3, 6 and 9 wt.%) on the EIS measurement was investigated at a constant current of 76 mA cm^{-2}. The fuel stoichiometric rate of the anode at the different methanol concentrations was set to 6. The cell was operated at 60 °C at a stoichiometric air flow rate at the cathode of 6. At

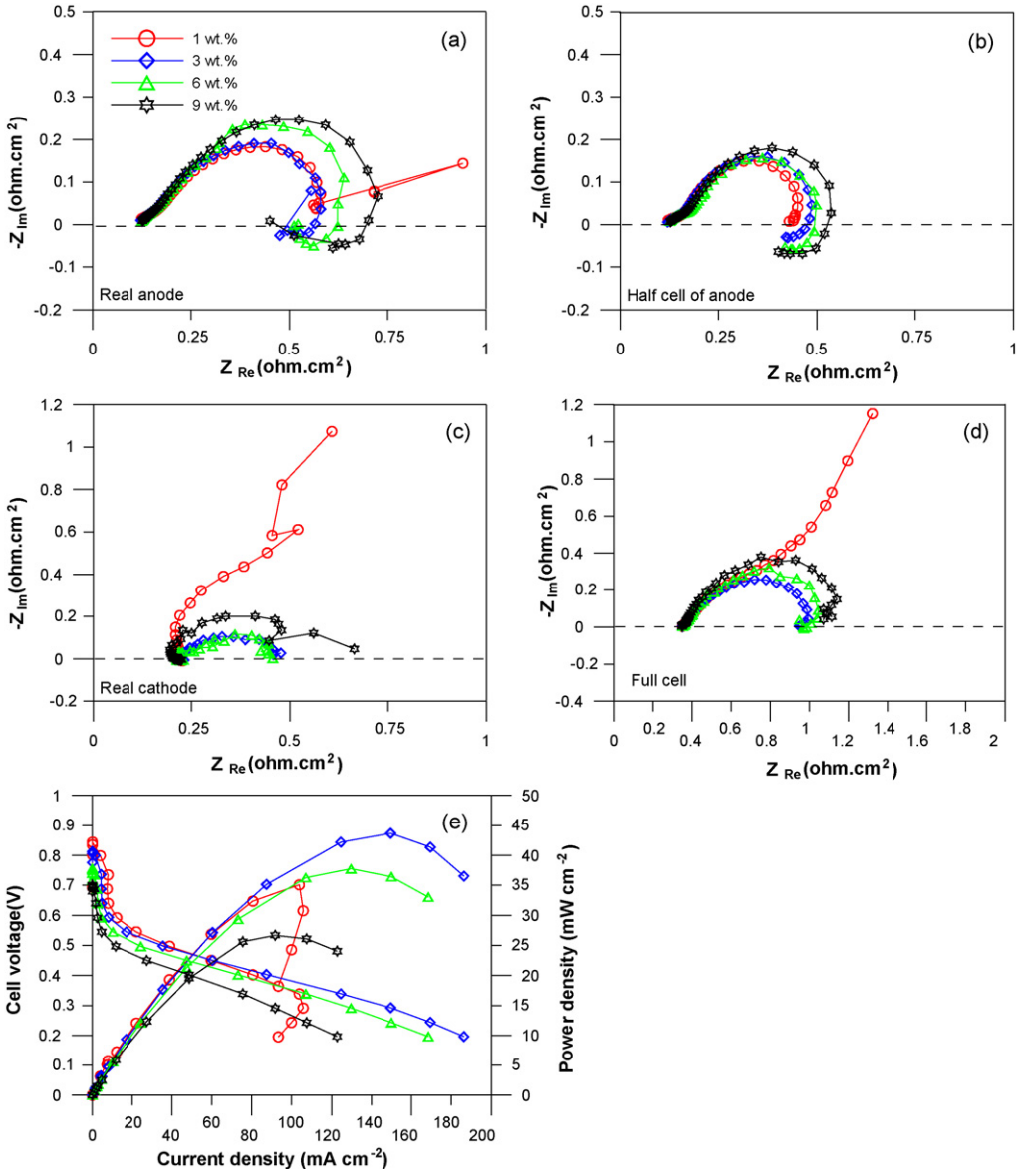

Fig. 9. The influence of 1, 3, 6 and 9 wt.% methanol concentrations on the EIS of (a) real anode, (b) half-cell of anode, (c) real cathode, (d) full cell, and (e) polarization curves. Cell temperature is 60 °C, both the anode and cathode flow are 6-stoichiometry.

the lowest methanol concentration (1 wt.%), Fig. 9(a) demonstrates that the effects of the mass-transport limitations on the anode EIS in the low-frequency region were similar to the conventional behaviors [2,3,7,12,18]. When the methanol concentration was increased to 3 wt.%, the MOR was enhanced by the decreased mass-transport limitation. Consequently, the CTR of the anode impedance decreased and an inductive part, corresponding to the adsorption step, appeared. As the methanol concentration was increased to 6 and 9 wt.%, the CTR of the anode impedance increased as well as the inductive part because a large amount of intermediate adsorbates reduced the active area of the anodic catalyst surface. Similar electrochemical behaviors were exhibited in the half-cell impedance of the anode, as shown in Fig. 9(b). Regarding the real-anode EIS, the real-cathode impedance is shown in Fig. 9(c). The large, irregular cathode impedance observed at 1 wt.% methanol reveals the restriction on the ORR, since the low methanol concentration strongly limited the transport of protons and electrons to the cathode side. As the methanol concentration increased, the transport of protons and electrons also increased. Therefore, the fast ORR caused the lower CTR in the cathode impedance observed at 3 wt.%. When the concentration was increased to 6 wt.%, no significant variations in real-cathode impedance were observed. However, the CTR significantly increased at a concentration of 9 wt.% because the excess methanol crossed the membrane and was oxidized at the cathode, thus reducing the efficiency of utilization by the catalyst [27,28]. Hence, the ORR was suppressed, which significantly impeded the real cathode, as shown by a second arc in the low-frequency region.

Fig. 9(d) shows the full-cell impedance spectra at various methanol concentrations. The large impedance arc was caused by the summing effect of both the limited MOR and the slow ORR at a concentration of 1 wt.%. Both the MOR and the ORR were improved at a concentration of 3 wt.%, thus reducing the CTR of the full-cell impedance. At a concentration of 6 wt.%, the large amount of intermediate adsorbates increased the CTR and the inductive part appeared. When the concentration was increased to 9 wt.%, methanol crossover resulted in a high CTR of the full-cell impedance with an irregular shape in the low-frequency region. The effect of methanol concentrations on the polarization curves associated with the full-cell EIS is plotted in Fig. 9(e). The low cell performance

reveals the mass-transport problem in the high current density region at a concentration of 1 wt.%. At a concentration of 3 wt.%, the reduced concentration polarization improved cell performance at high current density. However, diminishing cell performance was observed as the concentration was increased from 6 to 9 wt.%, because the high methanol concentration caused more methanol to be oxidized at the cathode side, leading to a drop in cell performance [16].

3.4. Effect of operating temperature

The influence of the operating temperature (30, 50 or 70 °C) on EIS measurement was evaluated at a constant current of 76 mA cm^{-2}. The stoichiometric flow rates of both methanol (3 wt.%) and air were 6. Fig. 10(a) displays the variation of the electrochemical behavior, as revealed by the real-anode impedance spectra, with temperature. The slow kinetics of the MOR at 30 °C is responsible for the large diameter of the real-anode impedance arc. As the cell temperature was increased to 50 °C or 70 °C, the kinetics of MOR were enhanced, thereby reducing the CTR of the real-anode impedance. Hence, the appearance of the inductive part indicates that the fast anode reaction generated a large amount of intermediate adsorbates on the catalyst surface. Additionally, the observation that the inductive part at 70 °C was smaller than that at 50 °C indicates that the adsorbed CO (CO_{ads}) desorption rate increased with the cell temperature. Furthermore, the decreased HFR of the real-anode impedance arc may result from the drop in electrical resistance of the MEA component at high temperature. Similar behaviors of the half-cell impedance of the anode are also presented in Fig. 10(b).

The high CTR of the real-cathode impedance shown in Fig. 10(c) reveals the depressed kinetics of ORR at 30 °C. As the temperature was increased, the HFR of the real-cathode impedance decreased and the enhanced cathode kinetics reduced the CTR as well. Although methanol and water crossover increased with the cell temperature [6,7], methanol crossover and water flooding did not

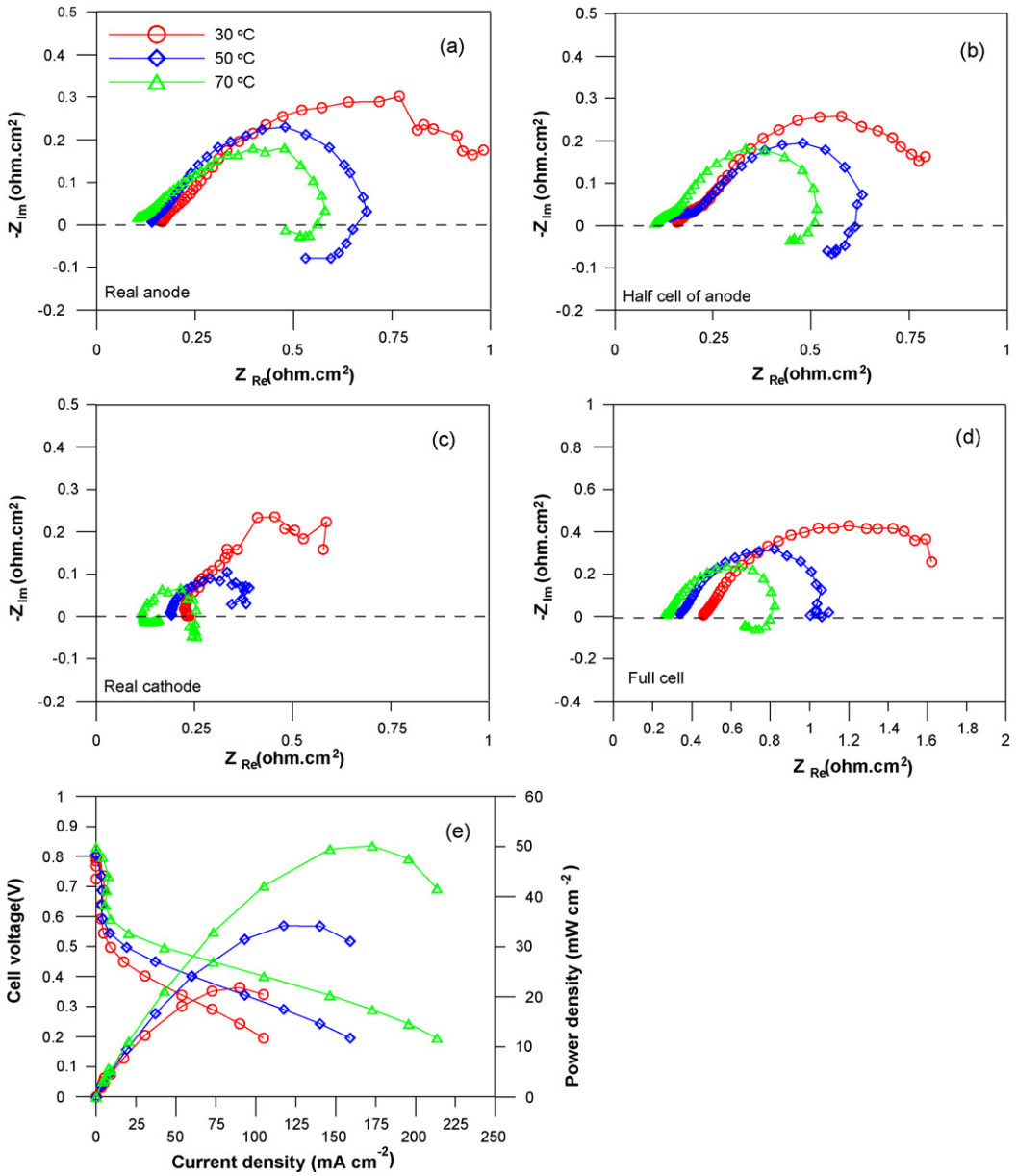

Fig. 10. The influence of cell temperatures (30, 50 and 70 °C) on the EIS of (a) real anode, (b) half cell of anode, (c) real cathode, (d) full cell, and (e) polarization curves. 3 wt.% liquid methanol is used, both the anode and cathode flow are 6-stoichiometry.

significantly affect the cathode impedance spectrum in our experiment. In the overall reaction, the full-cell EIS correlated with the polarization curves (Fig. 10(e)), as is shown in Fig. 10(d). The poor cell performance (Fig. 10(e)) due to the slow MOR and ORR at 30 °C produced high CTR of the full-cell impedance. As the temperature increased, the faster kinetics of both MOR and ORR reduced the CTR of the full-cell impedance. Again, the low HFR results in a decrease in the electric resistance as the temperature increases, as mentioned above. Therefore, both the enhanced kinetics and the lower ohmic losses significantly improved cell performance at 50 °C and 70 °C (Fig. 10(e)). Moreover, the inductive parts associated with full-cell impedance was not observed at 50 °C because of the cathode-diffusion problem, as described above (Fig. 10(d)). Although methanol and water crossover increased with cell temperature, they did not significantly affect the high cell performance at 70 °C or the EIS measurement.

3.5. Effect of operating-current density

The electrochemical behavior at three different current densities of 20, 40 and 76 mA cm^{-2} was evaluated at a cell temperature of 60 °C. The stoichiometric flow rates of both the 3 wt.% methanol and air supply corresponding to the operating current were set at 6 to eliminate mass-transfer limitations. Therefore, this experiment was performed under almost pure kinetic control. The current densities corresponding to the cell operating voltages in the polarization curves are shown in Fig. 11(a). For the full-cell impedance measurement, the charge-transfer processes reveal that both the CTR and inductive part decreased with increasing-current density [2–4,9,14,15,23,24], as is shown in Fig. 11(b). Fig. 11(c) shows that the slow kinetics of MOR caused the high CTR of the real-anode impedance, with a strong inductive effect at the low current density of 20 mA cm^{-2}. As the current density increased, both the CTR and

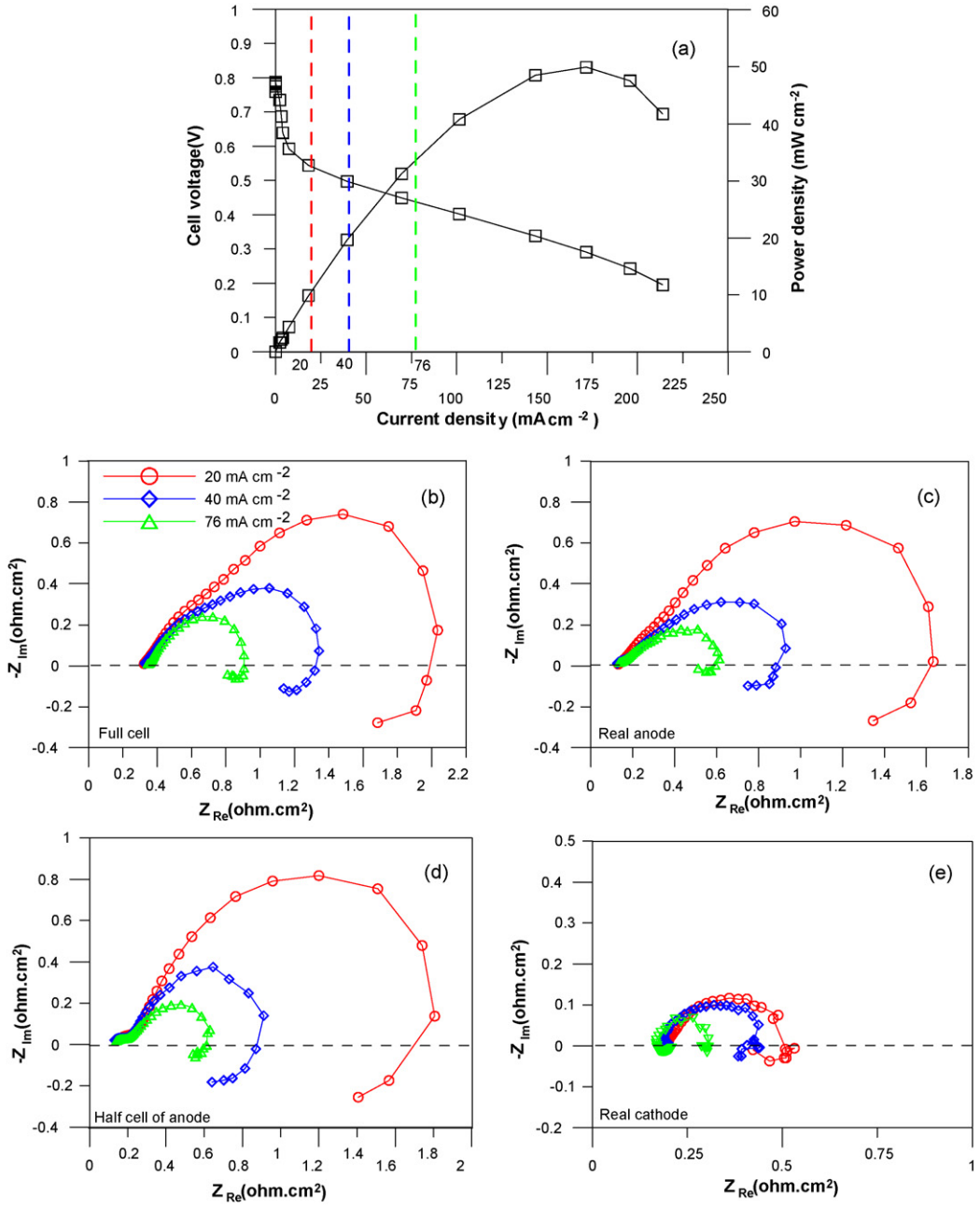

Fig. 11. The influence of various current densities (20, 40 and 76 mA cm^{-2}) on (a) polarization curves, (b) full cell impedance, (c) real-anode impedance, (d) half-cell impedance of anode, and (e) real-cathode impedance. Cell temperature is 60 °C, 3 wt.% liquid methanol is used, both air and methanol flow are 6-stoichiometry.

an inductive part of the real-anode EIS decreased. These decreases result from the enhanced kinetics of MOR, which accelerated the desorption rate of CO_{ads}. At a current density of 76 mA cm^{-2}, the adsorbed CO was quickly converted to CO_2 as a final product. Therefore, the small amount of CO_{ads} formed on the catalyst surface caused the almost complete disappearance of inductive behaviors. Similar electrochemical behaviors were obtained in the half-cell impedance of the anode, as is shown in Fig. 11(d). For the real cathode, the electrochemical behaviors as a function of the current density are shown in Fig. 11(e). At a current density of 20 mA cm^{-2}, the limited transport of both protons and electrons restricted ORR kinetics, leading to a large impedance arc in which the appearance of an inductive part may be due to methanol crossover or adsorbed intermediates on the cathode [2,3,23]. As the current density increased, the fast MOR enhanced the methanol consumption rate and reduced methanol crossover to the cathode. Moreover, fast transport of both protons and electrons also enhanced the kinetic ORR and the intermediate desorption rate. Therefore, the impedance spectrum at 76 mA cm^{-2} shows a small arc with a little inductive part.

3.6. Effect of flooding

To investigate the influence of cathode flooding on electrochemical behaviors, the EIS measurements associated with the polarization curves displayed in Fig. 12 were made at 76 mA cm^{-2}. The stoichiometric flow rates of both the 3 wt.% methanol and the air supply were 6 at a cell temperature of 60 °C. The impedance spectra, including those of the real cathode (Fig. 12(a)), the real anode (Fig. 12(b)), the full cell (Fig. 12(c)), and the half-cell anode (Fig. 12(d)), associated with the polarization curves (Fig. 12(e)) indicate that the cell was working effectively without any mass-transport problems in the initial state.

During a short-term test at 76 mA cm^{-2} for 155 min under the described operation conditions, cell performance was evaluated and HFR (1 kHz) was measured (Fig. 13). After 120 min, the performance, corresponding to the cell voltage, was unstable because the excess water blocked the pores of the GDL and restricted the transfer of oxygen. After a 160-min short-term test, the large impedance of the real cathode with an irregular shape in the low-frequency region indicates that water flooding occurred (Fig. 12(a)).

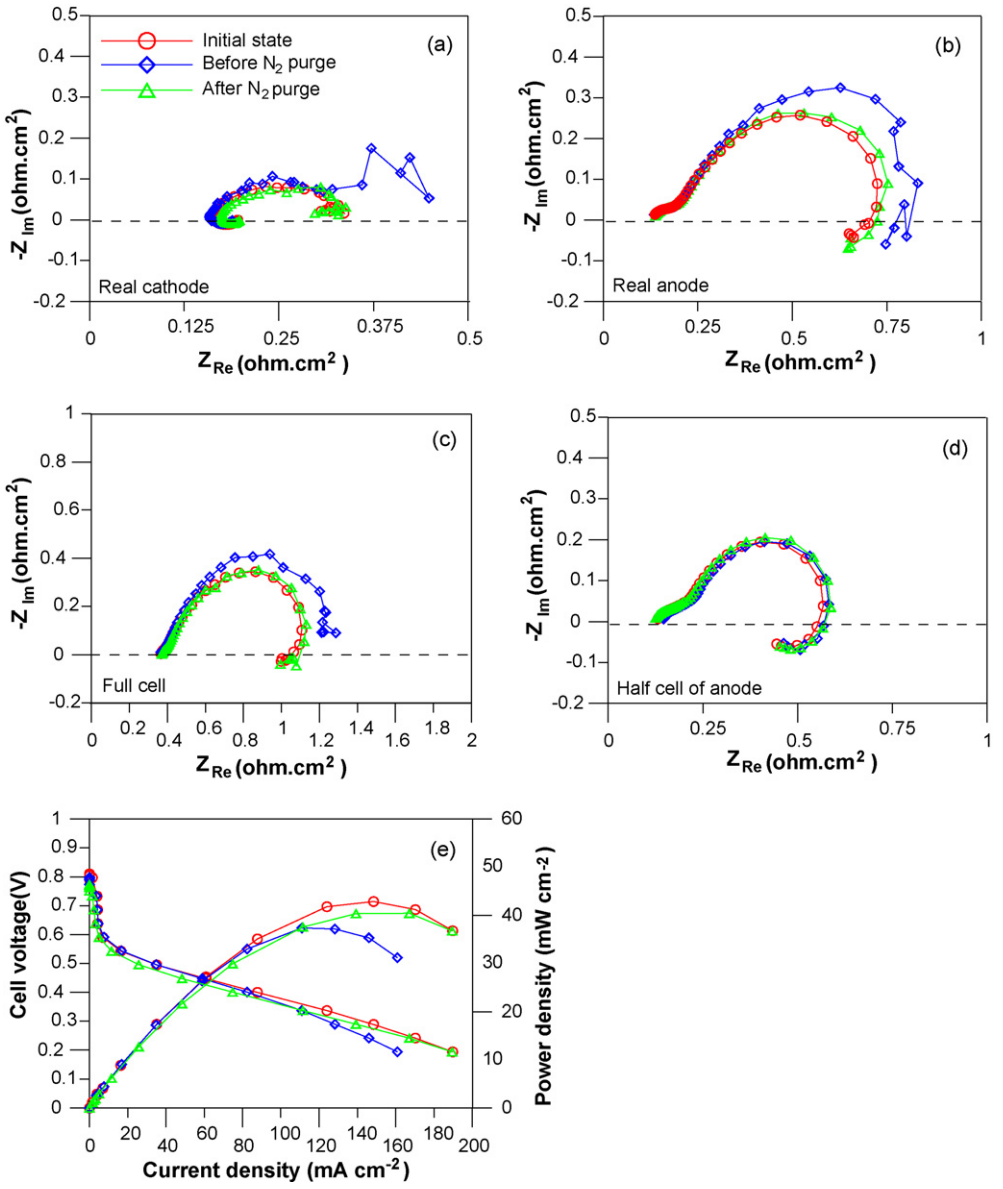

Fig. 12. The influence of cathode flooding on the EIS of (a) real cathode, (b) real anode, (c) full cell impedance, (d) half cell of anode, and (e) polarization curves. Cell temperature is 60 °C, 3 wt.% liquid methanol is used, both air and methanol flow are 6-stoichiometry.

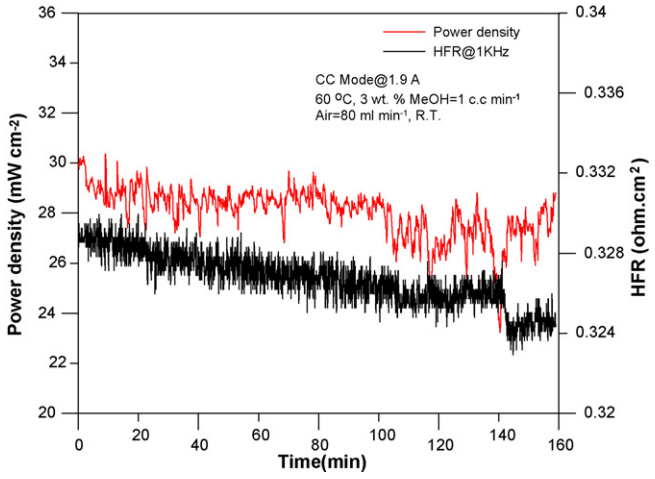

Fig. 13. The 160-min short-term test.

However, variation of the HFR was only approximately 1%, as is shown in Fig. 13. Since the membrane and anode were in contact with an aqueous solution, thereby ensuring maximum conductivity, the influence of water flooding on the HFR of DMFCs was not as clear as that in PEM fuel cells [36,37]. Since the reduction of oxygen transport due to water flooding slowed the proton-transfer process, the EIS of the real anode resulted in a large impedance arc (Fig. 12(b)). Therefore, the anode and cathode together were responsible for the high CTR of the full-cell impedance, with significant mass-transport limitations in the low-frequency region (Fig. 12(c)), and for low peak power at high current density in the polarization curve (Fig. 12(e)). However, the half-cell impedance of the anode did not vary with the test time (Fig. 12(b)), suggesting that determination of the half-cell impedance of the anode neglects the effect of the cathode and pertains only to the ideal conditions of the anode reaction.

To eliminate the effect of water flooding, nitrogen was employed to purge the excess water from the cathode side. Fig. 12(a) shows visible improvement of the cathode impedance in the low-frequency region after the nitrogen purge, compared with that before the purge. Once the problem of water flooding was eliminated by purging, the cathode impedance exhibited characteristics similar to those observed in the initial state, as is shown in Fig. 12(a). Similar variation in the EIS measurement for the real anode and the full cell can also be observed in Fig. 12(b) and (c), respectively. As the EIS measurement indicates elimination of water flooding, Fig. 12(e) clearly shows recovery of cell performance in the polarization curves after the nitrogen purge.

4. Conclusions

In this study, an extended reference electrode was used to observe in situ impedance of the anode and cathode during the actual operation of a DMFC. The sum of the individual anode and cathode impedances was consistent with the full-cell impedance, indicating that the setup of the Ag/AgCl reference electrode provided a good metric of cell performance. Moreover, both the results of ICP and EDX indicate that leakage of chloride ions did not poison the catalyst in our experiment. Systematic analysis of the impedance and polarization curves of an operating DMFC were performed to monitor the effects of the air and methanol flow rates, the methanol concentration, the temperature, and the current density. The following conclusions were drawn:

1. As the conventional half-cell impedance measurements relate only to the single electrode reaction under ideal conditions, the mutual influences of the critical operating conditions on each electrode cannot be observed using a pseudo-DHE.
2. Suppression of the reaction rate of the anode or the cathode by mass-transport limitations limits the reaction rate on the opposite side. Therefore, operating conditions of low air or methanol flow, and low or high methanol concentration critically affect the full-cell impedance spectra and polarization curves.
3. During stable operation, the reaction kinetics is subject to the operating-current density or the cell temperature. Apparently, the desorption rate of CO_{ads} increases as the operating-current density or cell temperature increases and the inductance correlates with potential-dependent capacitance changes due to changes in adsorption.
4. After water flooding occurred in the short-term test, in situ impedance in the low-frequency region clearly distinguished the effects on the cell performance at each electrode and the complete cell, whereas these effects were not obvious by the HFR.

The in situ impedance of each electrode determined by the extended reference electrode provided a better understanding of the operating and failure mechanisms of water flooding. Moreover, the proposed approach will support research and development efforts to prevent deterioration of the key component, the MEA, to improve the performance and durability of fuel cells and finally to facilitate the commercialization of direct methanol fuel cells.

Acknowledgement

The authors would like to thank the institute of Nuclear Energy Research (INER) for financially supporting this research.

References

[1] J.P. Meyers, J. Newman, J. Electrochem. Soc. 149 (2002) A718–A728.
[2] J.T. Mueller, P.M. Urban, J. Power Sources 75 (1998) 139–143.
[3] J.T. Mueller, P.M. Urban, W.F. Holderich, J. Power Sources 84 (1999) 157–160.
[4] J.C. Amphlett, B.A. Peppley, E. Halliop, A. Sadiq, J. Power Sources 96 (2001) 204–213.
[5] J.P. Diard, N. Glandut, P. Landaud, B.L. Gorrec, C. Montella, Electrochim. Acta 48 (2003) 555–562.
[6] X. Wang, J.M. Hu, I.M. Hsing, J. Electroanal. Chem. 562 (2004) 73–80.
[7] H. Fukunaga, T. Ishida, N. Teranishi, C. Arai, K. Yamada, Electrochim. Acta 49 (2004) 2123–2129.
[8] T. Vidakovic, M. Christov, K. Sundmacher, Electrochim. Acta 49 (2004) 2179–2187.
[9] J.S. Lee, K.I. Han, S.O. Park, H.N. Kim, H. Kim, Electrochim. Acta 50 (2004) 807–810.
[10] X. Zhao, X. Fan, S. Wang, S. Yang, B. Yi, Q. Xin, G. Sun, Int. J. Hydrogen Energy 30 (2005) 1003–1010.
[11] K. Furukawa, K. Okajima, M. Sudoh, J. Power Sources 139 (2005) 9–14.
[12] A. Oedegaard, J. Power Sources 157 (2006) 244–252.
[13] W. Chen, G. Sun, J. Guo, X. Zhao, S. Yan, J. Tian, S. Tang, Z. Zhou, Q. Xin, Electrochim. Acta 51 (2006) 2391–2399.
[14] D. Chakraborty, I. Chorkendorff, T. Johannessen, J. Power Sources 162 (2006) 1010–1022.
[15] N.Y. Hsu, S.C. Yen, K.T. Jeng, C.C. Chien, J. Power Sources 161 (2006) 232–239.
[16] C.Y. Chen, P. Yang, Y.S. Lee, K.F. Lin, J. Power Sources 141 (2005) 24–29.
[17] C.Y. Chen, J.Y. Shiu, Y.S. Lee, J. Power Sources 159 (2006) 1042–1047.
[18] J. Lobato, P. Cañizares, M.A. Rodrigo, J.J. Linares, A.F. Fragua, Chem. Eng. Sci. 61 (2006) 4773–4782.
[19] H. Kima, S.J. Shin, Y.G. Park, J. Song, H.T. Kim, J. Power Sources 160 (2006) 440–445.
[20] T. Schultz, U. Krewer, T. Vidakovic, M. Pfafferodt, M. Christov, K. Sundmacher, J. Appl. Electrochem. 37 (2007) 111–119.
[21] M.K. Jeon, J.Y. Won, K.S. Oh, K.R. Lee, S.I. Woo, Electrochim. Acta 53 (2007) 447–452.
[22] C.Y. Du, T.S. Zhao, C. Xu, J. Power Sources 167 (2007) 265–271.
[23] C.Y. Du, T.S. Zhao, W.W. Yang, Electrochim. Acta 52 (2007) 5266–5271.
[24] K.T. Jeng, C.C. Chien, N.Y. Hsu, W.M. Huang, S.D. Chiou, S.H. Lin, J. Power Sources 164 (2007) 33–41.
[25] J. Zhang, G.P. Yin, Q.Z. Lai, Z.B. Wang, K.D. Cai, P. Liu, J. Power Sources 168 (2007) 453–458.
[26] J.K. Lee, J. Choi, S.J. Kang, J.M. Lee, Y. Tak, J. Lee, Electrochim. Acta 52 (2007) 2272–2276.

[27] S.R. Narayanan, A. Kinder, B.J. Nakamura, W. Chun, H. Frank, M. Smart, T.I. Valdez, S. Surampudi, G. Halpert, J. Kosek, C. Cropley, Annu. Battery Conf. Appl. Adv. 11 (1996) 113–122.
[28] H. Dohle, J. Divisek, J. Mergel, H.F. Otjen, C. Zingler, D. Stolten, J. Power Sources 105 (2002) 274–282.
[29] X. Ren, T.E. Springer, S. Gottesfeld, J. Electrochem. Soc. 147 (2000) 92–98.
[30] A. Kuver, I. Vogel, W. Vielstich, J. Power Sources 52 (1994) 77–80.
[31] A. Kuver, W. Vielstich, J. Power Sources 74 (1998) 211–218.
[32] S. Mitsushima, N. Araki, N. Kamiya, K. Ota, J. Electrochem. Soc. 149 (2002) A1370–A1375.
[33] T.E. Springer, M.S. Wilson, S. Gottesfeld, J. Electrochem. Soc. 140 (1993) 3513–3526.
[34] S. Enback, G. Lindbergh, J. Electrochem. Soc. 152 (2005) A23–A31.
[35] Y. Kim, W. Hong, S. Woo, H. Lee, J. Power Sources 159 (2006) 491–500.
[36] T.E. Springer, T.A. Zawodzinkski, M.S. Wilson, S. Gottesfeld, J. Electrochem. Soc. 143 (1996) 587–599.
[37] J.O. Schumacher, P. Gemmar, M. Denne, M. Zedda, M. Stueber, J. Power Sources 129 (2004) 143–151.
[38] P. Piela, T.E. Springer, J. Davey, P. Zelenay, J. Phys. Chem. C 111 (2007) 6512–6523.
[39] Z. Liu, J.S. Wainright, W. Haung, R.F. Sacinell, Electrochim. Acta 49 (2004) 923–935.
[40] M. Seo, Y. Yun, J. Lee, Y. Tak, J. Power Sources 159 (2006) 59–62.
[41] S. Uhm, T. Noh, Y.D. Kim, J. Lee, Chemphyschem 9 (2008) 1425–1429.
[42] X. Zhao, G. Sun, L. Jiang, W. Chen, S. Tang, Q. Xin, Electrochem. Solid-State Lett. 8 (2005) A149–A151.
[43] S. Eccarius, T. Manurung, C. Ziegler, J. Electrochem. Soc. 154 (2007) B852–B864.